

Student-led Design, Construction, and Testing of a Permanent Magnet Hall Thruster on Argon Propellant

Ari J. Eckhaus *, Adrian J. Rocha**, Andrew M. Saladino**, and Benjamin A. Jorns ‡

Department of Aerospace Engineering, University of Michigan, Ann Arbor, MI, 48104

In this project, a team of undergraduate students worked to design, construct, and test a permanent magnet Hall-Effect Thruster that operated on argon gas propellant. This thruster was intended to be presented as a demonstration of electric propulsion at future K-12 outreach events. Over the course of one semester the thruster design was validated through simulation and a virtual interface was created with the PEPL MAISE vacuum facility. Utilizing accessible manufacturing techniques and outsourcing parts when necessary, the thruster was manufactured for less than \$2000. Ultimately, the thruster was able to achieve ignition on argon.

I. Nomenclature

<i>HET</i>	= Hall-Effect Thruster
<i>EP</i>	= Electric Propulsion
<i>PEPL</i>	= Plasmadynamics and Electric Propulsion Laboratory
<i>MAISE</i>	= Michigan Advanced In-Space propulsion Engineers
<i>MFC</i>	= Mass Flow Controller
<i>r_L</i>	= Larmor Radius [m]
<i>L</i>	= Channel Length [m]
<i>m</i>	= Mass of Electron [kg]
<i>e</i>	= Charge of Electron [C]
<i>B</i>	= Magnetic Field Strength [G]
<i>T_{eV}</i>	= Electron Temperature [eV]
<i>M</i>	= Mass of Ion [kg]
<i>V_b</i>	= Anode Voltage [V]
<i>λ_i</i>	= Mean Free Path Length [m]
<i>v_n</i>	= Neutral Velocity [m/s]
<i>n_e</i>	= Electron Number Density [m ⁻³]
<i>σ_iv_e</i>	= Reaction Rate Coefficient [m ³ s]
<i>v_{Xe}</i>	= Neutral Velocity of Xenon [m/s]
<i>m_{Xe}</i>	= Mass of Xenon Atom [kg]
<i>v_{Ar}</i>	= Neutral Velocity of Argon [m/s]
<i>m_{Ar}</i>	= Mass of Argon Atom [kg]
<i>p</i>	= Fraction of Neutral Atoms to be Ionized
<i>K</i>	= Kinetic Energy [J]
<i>f_c</i>	= Cutoff Frequency [Hz]
<i>R</i>	= Resistance [Ω]
<i>C</i>	= Capacitance [F]

*Ph.D. Precandidate, Department of Aerospace Engineering, University of Michigan, Ann Arbor, MI, 48104

**MSE Student, Department of Aerospace Engineering, University of Michigan, Ann Arbor, MI, 48104

***MSE Student, Department of Aerospace Engineering, University of Michigan, Ann Arbor, MI, 48104

‡AIAA Associate Fellow, Department of Aerospace Engineering, University of Michigan, Ann Arbor, MI, 48104

II. Introduction

In 1971, the Meteor satellite launched from the Soviet Union. On board, the satellite contained a new experimental "Stationary Plasma Thruster", intended to prove that electric thrusters could achieve steady state operation in space. In the five decades since, the Stationary Plasma Thruster has become better known as the Hall-Effect Thruster, and the technology has become the most common form of electric propulsion flown in space. As such, the Hall thruster has also been a key subject of interest for electric propulsion research institutions, such as the University of Michigan's Plasmadynamics and Electric Propulsion Laboratory (PEPL).

While electric propulsion is a growing area of research, many of the fundamental concepts of EP are inaccessible at the undergraduate level. Additionally, the necessity of vacuum chambers and high-power electrical supplies for thruster testing further limits access to EP. To date, only a select number of undergraduate students have completed a full design and test cycle of a Hall-Effect Thruster. In 2016-2017, Matthew Baird, at Western Michigan University (WMU), designed and tested a thruster that achieved ignition on xenon [1, 2]. In 2020, a team of students based out of Olin college started working with Hall thrusters. In the time since, they have designed several devices, one of which utilized permanent magnets and was designed to operate on argon [3, 4]. At the University of Michigan, in an attempt to provide a pathway for undergraduate students to work with EP technologies, PEPL created the undergraduate student team, Michigan Advanced In-Space Propulsion Engineers (MAISE). The goal of MAISE is to create small-scale demonstration thrusters that can be brought to outreach events to generate excitement about EP and spaceflight. Currently, MAISE has a working pulsed plasma thruster (PPT) and a small-scale Hall thruster. This thruster, while functional, is over 25 years old and has proven to be unreliable during demonstration events.

As a way to gain more hands-on experience with EP, we formed a team of three students to design, build and test a replacement Hall thruster over the course of a semester. The intention was for the replacement thruster to operate at similar power levels to the current device (approximately 200 W), but utilize permanent magnets to supply the thruster's magnetic field. We also wanted to use argon propellant instead of traditional xenon or krypton since these traditional propellants are prohibitively expensive for a demonstration thruster.

With these goals in mind, this paper is organized in the following way. In the first section, we overview the Hall thruster principle of operation and the design principles and scaling laws that we leveraged for our design. In the second section, we introduce a preliminary design and walk through the iterative design process. In the third section, we discuss the construction of the thruster utilizing in-house and external manufacturing resources. In the fourth section, we explain the experimental setup for testing the thruster in the existing MAISE vacuum facility along with the interfacing for remote control and data acquisition purposes. In the fifth section, we examine the thruster performance results during and after ignition. In the final section, we have a high-level discussion of our results in relation to Hall thruster inefficiencies and lifetime.

III. Scaling Laws for Informing Thruster Design

A. Hall Thruster Principle of Operation

Fundamentally, the Hall-Effect Thruster relies upon the electrostatic potential between a negatively charged cathode and positively charged anode to accelerate ions. As we show below in a quarter section of the canonical Hall thruster geometry in Figure 1, the anatomy of a Hall thruster consists of a hollow cathode, an anode, an annular channel, and a magnetic circuit. The hollow cathode, often placed just adjacent to the thruster's channel, acts as an electron source. The anode, located at the base of the channel, attracts the electrons emitted by the cathode and creates an axial electric field in the channel. The magnetic circuit is designed such that there is an approximately radial magnetic field across the channel, perpendicular to the electric field. As electrons travel from the cathode to the anode, they interact with the radial magnetic field. Rather than freely passing to the anode, electrons begin to orbit the magnetic field lines. As electrons orbit the magnetic field lines, they experience an $\mathbf{E} \times \mathbf{B}$ drift, creating an azimuthal current. This drift is caused by a phenomenon known as the Hall effect, from which the thruster derives its name. A neutral gas, often xenon or krypton, is then injected into the channel by a gas distributor positioned at the channel base. The azimuthal current of electrons collides with the neutral gas particles, resulting in ionization. The ions are then accelerated by the applied electric field and neutralized downstream by electrons pulled from the cathode. The electrons resulting from ionization join the azimuthal Hall current to continue the ionization process in a phenomenon of "avalanche ionization", contributing to the high efficiencies of Hall thrusters. Locally, the acceleration of ions takes place in a quasi-neutral

plasma, such that there is no space charge limitation that inhibits the thrust density. In comparison to other electric propulsion devices like gridded ion thrusters, Hall thrusters have a high thrust density. The acceleration of ions is inherently electrostatic, so the specific impulse scales with the applied electric field. On xenon propellant, Hall thrusters can reach a specific impulse higher than 3000 seconds.

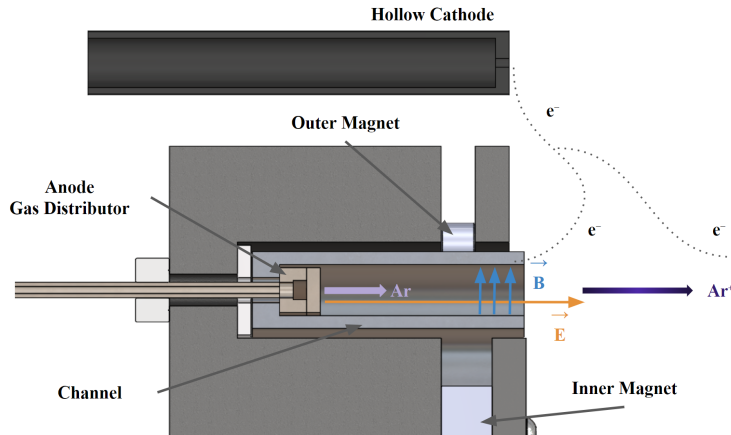


Fig. 1 A Quarter Section of Canonical Hall Thruster Geometry

B. Design Space

The general design for the Hall thruster, including components, scaling laws, and other theoretical topics were largely derived from Fundamentals of Electric Propulsion by Goebel & Katz [5].

The theory provided by Goebel & Katz leaves a rather large design space that must be narrowed. Though choosing a permanent magnet architecture somewhat simplifies the design process, the remaining variables in the space include magnet dimensions and material, channel length, soft iron dimensions, and the possibility of adding mu metal screens. To cut this space down, these variables were simplified to the magnet diameter and thickness, height of magnets from the anode, and outer magnet radial position.

An iterative design process was undertaken using a 2-D COMSOL Multiphysics simulation. A preliminary sketch with arbitrary dimensions similar to the thruster used by MAISE, the PEPL-70, was drafted, and the aforementioned variables were modified to ascertain general trends. It was found that the magnetic field peak distance from the anode essentially followed the outer magnet distance from the anode. It was also found that moving the outer magnets radially outward decreased the peak field strength and vice versa. Additionally, it was found that changing the height of any magnet did not significantly affect the field, but changing the diameter had an effect. Increasing the inner magnet width weakened the field at most locations, while increasing the outer magnet widths strengthened it.

C. Magnetic Field Strength

An estimate for the peak magnetic field strength required in the Hall thruster channel was determined based on constraints on the electron and ion Larmor radii. These radii are inversely proportional to the magnitude of the peak B-field strength and thus constrain it.

1. Electron Larmor Radius

The Larmor radii of both electrons and ions around the magnetic field can be used to provide a general range for the maximum B-field strength. Equation 1 can be used to calculate the Larmor radius of electron paths around the magnetic field lines near the end of the channel.

$$r_L = \frac{1}{B} \sqrt{\frac{8m}{\pi e} T_{eV}} \ll L \quad (1)$$

L represents the channel length, r_L is the Larmor radius, B is the magnetic field strength, m is the mass of an electron, e is the charge of an electron, and T_{eV} is the electron temperature in electronvolts. Electron temperatures in Hall thruster channels typically fall in the range of 20-50 eV [6][7]. The Larmor radius calculated in the paper from the WMU team was 2.5 mm, and the Larmor radius of the archetypal Hall thruster example in Goebel & Katz was 1.3 mm.

Expanding this range slightly and using a range of 1-3 mm for the Larmor radius and 20-50 eV for the electron temperature allows us to find a lower and upper range for the B-field strength. A large Larmor radius and low electron temperature gives a low B-field strength and vice-versa. The resulting B-field strength range evaluates to roughly 60-250 G.

The primary requirement for the electron Larmor radius is that it is significantly smaller than the thruster's characteristic channel length. This length is around 5 cm for this thruster. Thus, the Larmor radius can safely be smaller than 1 mm as long as it does not significantly decrease the Larmor radius of the ions. The Larmor radius is decreased when B-field strength is increased, so a B-field strength above 250 G could be acceptable within a certain limit.

2. Ion Larmor Radius

The Larmor radius of argon ions can be calculated using Equation 2:

$$r_L = \frac{1}{B} \sqrt{\frac{2M}{e}} V_b \gg L \quad (2)$$

Here, M is the mass of the ion (argon's atomic mass in this case), V_b is the anode voltage, and the other variables are the same as in the equation above. Assuming a voltage of 400 V, the Larmor radius with a B-field range of 60-250 G is 0.7-3.0 m. The B-field strength can be increased as long as the Larmor radius of the ions does not shrink enough that it becomes close to the characteristic length of the thruster. If the ion Larmor radius becomes too short, then there is a risk that ions will be significantly perturbed azimuthally on their way through the channel.

Using a safety factor of 2.0, a minimum ion Larmor radius of 10 cm can be defined. Substituting this back into Equation 2 above, it can be calculated that this corresponds to a maximum B-field strength of 1820 G. These calculations define a range of around 60-1800 G for the maximum B-field strength near the end of the channel. However, most small Hall thrusters have field strengths on the order of the lower hundreds and not thousands of Gauss, so a strength of roughly 200-300 G was targeted.

D. Thruster Radius

Few initial constraints were placed on the initial thruster radius. As a starting point, we chose a similar thruster diameter to the PEPL-70 (approximately 3 inches). During the iterative design process using COMSOL, the radial and axial position of the single outer magnet in a 2-D simulation was adjusted to optimize the B-field shape. This process is expanded on further in the discussion on the iterative design procedure later in this paper. The outer magnet position that produced a radial B-field near the channel exit and led to the desired ionization region thickness was used to inform the final thruster radius. The radius of the thruster was chosen to be slightly larger than the outer edge of the outer magnet at its position in the simulation. The size of this small margin was chosen somewhat arbitrarily and the thruster radius was ultimately set to exactly 2.5 inches for ease of machining.

E. Channel Length

The length of the thruster channel was determined chiefly based on the fact that the thruster was designed to run on argon propellant. Argon is less massive and has a higher ionization energy than conventional Hall thruster propellants like xenon and krypton. A simple scaling argument was used to contrast this thruster with thrusters designed to run on other propellants; specifically, that ionization region length scales proportionally to propellant velocity and inversely to ionization cross-section.

1. Ionization Length for Xenon

To find the length of an argon-fueled thruster's channel, the ionization length of a xenon-fueled Hall thruster was estimated, and the aforementioned scaling argument was applied to convert this into an ionization length for an argon-fueled thruster. Then, this length was added to the distance from the anode that the strongest region of the field

needed to be located to achieve near-zero B-field at the anode (defining “near-zero” as less than 5 G). This second distance was determined using COMSOL simulations of the thruster design.

The ionization region length estimate for a xenon-fueled thruster is based firstly on an estimate of the ionization mean free path length and secondly on the fraction of neutral atoms which are to be ionized. This fraction is a parameter which can be set by the designer. Equation 3 below from Goebel & Katz was used to calculate the mean free path length using the neutral velocity of xenon v_n , electron number density n_e and reaction rate coefficient $\langle \sigma_i v_e \rangle$:

$$\lambda_i = \frac{v_n}{n_e \langle \sigma_i v_e \rangle} [5] \quad (3)$$

The neutral velocity of xenon at a given temperature can be estimated by using the equation for the mean thermal velocity using a Maxwell-Boltzmann distribution:

$$v_{Xe} = \sqrt{\frac{8kT}{\pi m_{Xe}}} [8] \quad (4)$$

Assuming room temperature (298 K), this evaluates to around 220 m/s for neutral xenon. Next, because it is difficult to calculate the number density of electrons in the ionization region from first principles, empirical data from the SPT-100 was utilized. According to the measurements, the number density n_e at the exit plane of the SPT-100 is roughly 10^{18} m^{-3} [9].

The ionization reaction rate coefficient for xenon was determined from a fit to a large body of empirical data taken as a function of electron thermal velocity. Assuming a thermal velocity of 35 eV, the reaction rate coefficient is $1.734 \times 10^{-13} \text{ m}^3/\text{s}$ [10].

Making use of these three values, the mean free path for xenon was estimated using Equation 3 above to be 1.27 mm. The ratio between the ionization region length and mean free path is determined by the fraction of neutral atoms that one intends to ionize, and increases as this fraction increases. Equation 5 below uses this relationship to calculate the length L of the ionization region:

$$L = -\lambda_i \log(1-p) [5] \quad (5)$$

where p is the fraction of neutral atoms to be ionized and λ_i is the mean free path of ionization. Using a fraction of 0.95 (as suggested in Goebel & Katz) and the mean free path for xenon calculated above, the ionization region length will be around 3.8 mm, or approximately 3 times the mean free path. This is a rough estimate of the ionization region length of a xenon Hall thruster with a similar design to the SPT-100.

2. Scaling for Argon

The scaling argument used to compare xenon and argon ionization lengths first requires the ratio of neutral velocities of xenon and argon to be determined. Assuming that an atom of xenon propellant has the roughly the same kinetic energy as an atom of argon propellant, this can be trivially determined from the equation for the kinetic energy of a moving body:

$$K = \frac{1}{2}mv^2 \quad (6)$$

$$m_{Xe}v_{Xe}^2 = m_{Ar}v_{Ar}^2 \quad (7)$$

$$\frac{v_{Ar}}{v_{Xe}} = \sqrt{\frac{m_{Xe}}{m_{Ar}}} \quad (8)$$

Using this relation, the ratio of the neutral velocities of argon and xenon is 1.81. The ionization cross sections of argon were determined using data tables which listed cross section as a function of electron thermal velocity. The values used were for 36 eV since the table did not contain values for 35 eV. The corresponding ratio between argon and xenon cross sections is 0.52 [11].

Since ionization length is directly proportional to neutral velocity and inversely proportional to ionization cross section, applying the scaling argument to the xenon ionization length gives the following value for the argon ionization length:

$$3.8 \text{ mm} \times \frac{1.81}{0.52} = 13.2 \text{ mm} \quad (9)$$

The ionization region's size can be estimated in a COMSOL simulation by looking at the region of strong B-field lines crossing the channel. Since the ionization region thickness is based on a rough estimate, it is sufficient to adjust parameters such as the magnet and soft iron positions in COMSOL to alter this thickness. The ionization region and its magnetic field must also be far enough from the anode so that a significant magnetic field is not generated there. This distance was also found iteratively using COMSOL simulations.

IV. Thruster Design

A. Magnetic Circuit

The thruster's magnetic circuit is responsible for both directing field lines radially across the channel, as well maintaining the appropriate field strength described in Section III.C. The primary magnetic field of our thruster is produced by permanent magnets, compared to commonly used electromagnets. The two commonly used types of permanent magnets are SmCo magnets and neodymium magnets. Neodymium magnets have a much stronger magnetic field and tend to be cheaper [12]. However, since we anticipate operating at high temperatures, we selected SmCo magnets since they don't lose their magnetic properties as quickly when the operating temperature is increased [13]. We determined that the magnetic field strength was optimal when 10 outer magnets were used and a single inner magnet. We utilized iron components to direct the magnetic field lines. Iron has a high magnetic permeability, meaning that the magnetic field freely passes through iron with less resistance than the surrounding materials. This allowed us to shape the magnetic field by changing the geometry of the iron parts. The final configuration resulted in a field strength of approximately 330 G at the channel centerline, peaking near the channel exit. The key components of the thruster magnetic circuit are shown in Figure 2.

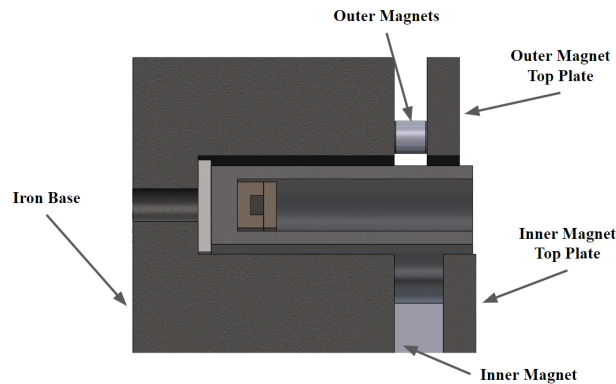


Fig. 2 Magnetic Circuit Quarter Section

1. Iterative Design Procedure

The dimensions of the permanent magnets, soft iron components and attached structural components were largely determined through an iterative simulation process in COMSOL. For the sake of simplicity, a 2-D radial simulation was used for this process. The simulation represented the cross-section on a plane running from the central axis of the thruster out to the edge — a rectangular region that would produce a representation of the entire thruster if revolved around the central axis.

The iterative design process began by drawing up a sketch of a Hall thruster design with largely arbitrary dimensions. The initial radius, for example, was 2.5", similar to the PEPL-70 thruster. Olin's permanent magnet thrusters placed the

magnets near the base of the channel [3]. However, this appeared to create an unwanted field near the anode, so we opted to place SmCo (Samarium Cobalt) magnets near the channel exit under the cross-sections of soft iron disks to guide the field radially. Using the scaling laws described earlier in Section III.B., the magnet dimensions and positions as well as soft iron dimensions were iteratively modified, first to achieve a magnetic field with a reasonable peak field strength (see section III.A.) and then a field with a roughly uniform shape. The first concrete design decision made was the magnet dimensions. As SmCo magnet dimensions are limited by the specific sizes provided by manufacturers, it was quite easy to iterate through the list of available sizes and observe their effects on the field shape in the COMSOL simulation. The favored choices were outer magnets with both a thickness and diameter of 0.25", and an inner magnet with a thickness of 0.375" and a diameter of 0.75".

2. 2-D Simulation

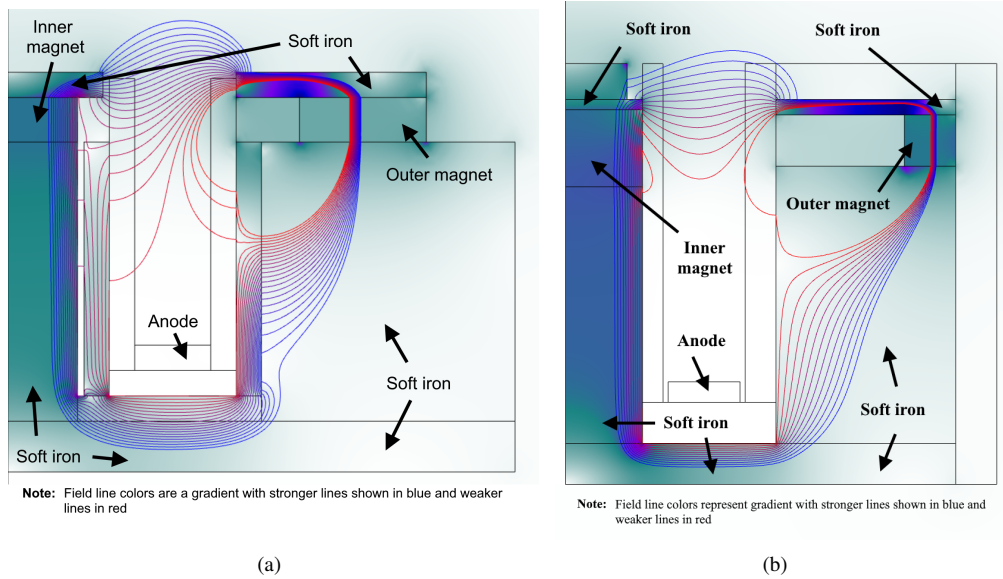


Fig. 3 (a) Early Iteration of 2-D COMSOL Design, (b) Final Design Iteration of 2-D COMSOL Simulation

Figure 3 (a) above shows a relatively early iteration of the 2-D simulation design. Note the field lines being directed through the soft iron components as intended, though they do not cross the channel in a uniform radial manner. This design dates to a point before the final magnet dimensions were chosen. Further improvements to the design worked to direct the strong B-field lines radially without any straying downward toward the lower channel walls.

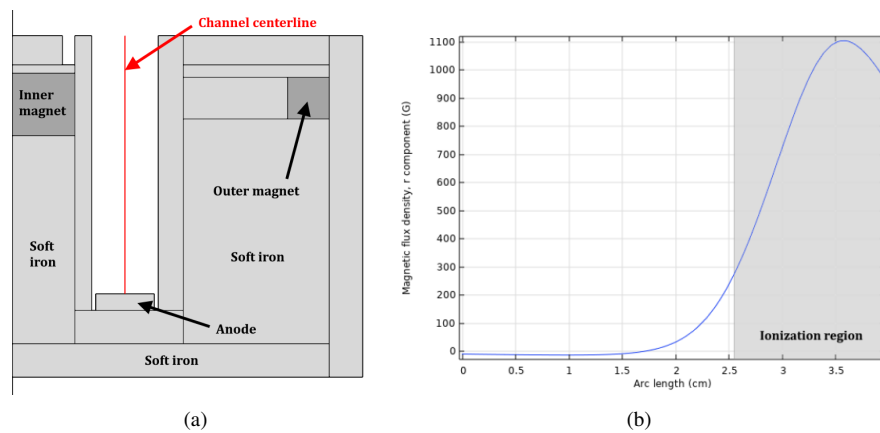


Fig. 4 (a) Channel Centerline View, (b) B-field Profile Along Centerline

The final design in the 2-D COMSOL simulation has a peak B-field strength of roughly 1100 G (see Figure 4), which is well above the 200-300 G target but within the 60-1800 G range determined earlier from scaling laws. As shown in Figure 3 (b), the B-field profile is roughly radial, particularly for the stronger (blue) lines. Note that the distance between the bottom and top radial lines is roughly 0.6", and this distance drops to 0.5" if the weakest (bottom) line is excluded. Using this distance as a rough estimate of the plasma thickness, it can be concluded that the ionization region roughly corresponds to the size derived from the previously discussed scaling laws.

3. 3-D Simulation

After the design goals related to plasma thickness, peak B-field strength and field shape were achieved, a 3-D model of the thruster equivalent to a revolved 2-D COMSOL model was generated using SolidWorks CAD software. A number of design changes were made when converting the 2-D simulation to the final CAD model, mostly for ease of manufacturing.

This modified 3-D design was imported into COMSOL, and its magnetic field was modeled. Notably, the final model has ten inner magnets placed at the same radius and evenly spaced azimuthally. The iron front plates above the inner and outer magnets serve to distribute the field equally in all directions. In principle, this allows the field to be azimuthally uniform around the channel, despite the outer field being generated by discrete permanent magnets. In reality, some azimuthal variation was observed from the 3-D simulation. Since the thruster components were placed to optimize the field at cross sections centered on the outer magnets, the fields at cross-sections centered between magnets have the least optimal shape (i.e. the field lines are the least radial). The fact that the final thruster design differs somewhat from the optimized 2-D design for manufacturability also contributed to slight warping of the field shape. Nonetheless, COMSOL simulations showed that the field shape is still quite functional. This is illustrated in Figure 5. Though a number of field lines do not follow a strictly radial direction, this occurs in a region where the B-field is comparatively weak, and the lines in the region with a strong B-field overwhelmingly point in a radial direction.

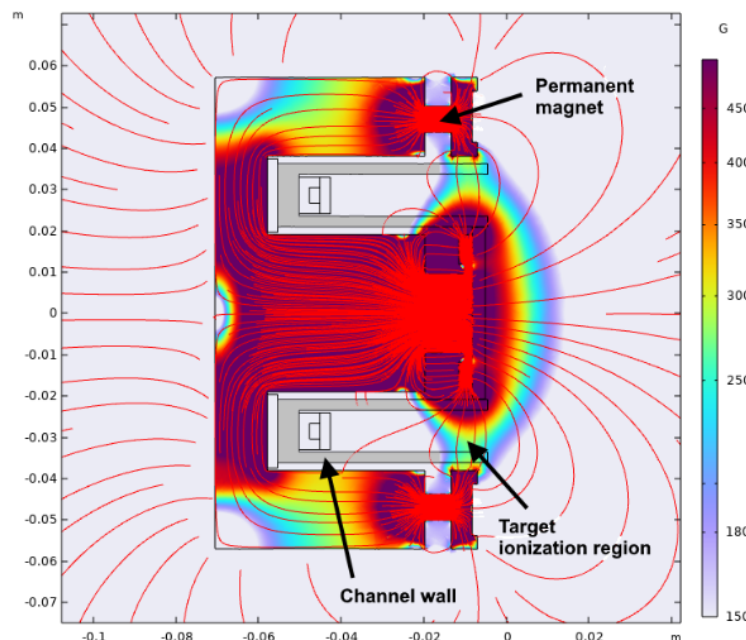


Fig. 5 3-D Simulation Cross-sectional B-field

It is important to note that the maximum B-field value of 1100 G for the 2-D simulation is not representative of the maximum B-field strength in the final 3-D simulation. This is because of the differences in geometry between the 3-D and 2-D simulations — in the 3-D simulation, the B-field generated by each magnet spills into the regions between the magnet cross-sectional "slices". The maximum B-field along the channel centerline in the 3-D simulation was roughly 330 G — much closer to the 200-300 G benchmark outlined earlier.

4. Finalized Design and Construction

In our thruster design, we used an iron base to direct the magnetic field behind the channel. This was necessary to minimize the magnetic field at the anode. The base also required areas for propellant and electrical lines to pass through, while remaining isolated. This was accomplished using ceramic standoffs, which insulated the propellant lines going to the anode. At the exit plane of our thruster, we designed two iron top plates to sit above the inner magnet and outer magnet array. These top plates helped direct the field lines across the channel, effectively completing the magnetic circuit, and ensuring that the field peaked near the exit plane. A quarter section view of the magnetic circuit is shown in Figure 2.

5. Comparison of Magnetic Field Map with Simulation

To both better characterize the thruster and determine agreement with the simulated magnetic field topology, we utilized the PEPL magnetic field mapper to measure strength of the field along the channel center line. The mapper consists of a Hall sensor mounted to a three axis motion stage, allowing for precise measurements of magnetic field strength and direction. To take the measurement, the channel and anode were removed from the thruster, ensuring that the magnetic circuit was complete, but allowing clearance for the Hall sensor. The probe was swept from the channel exit plane to the nominal anode location, measuring the radial and axial field at 1 mm increments. We present below the results of the field mapping showing the radial and axial components of the magnetic field along the channel center-line as well as the field magnitude.

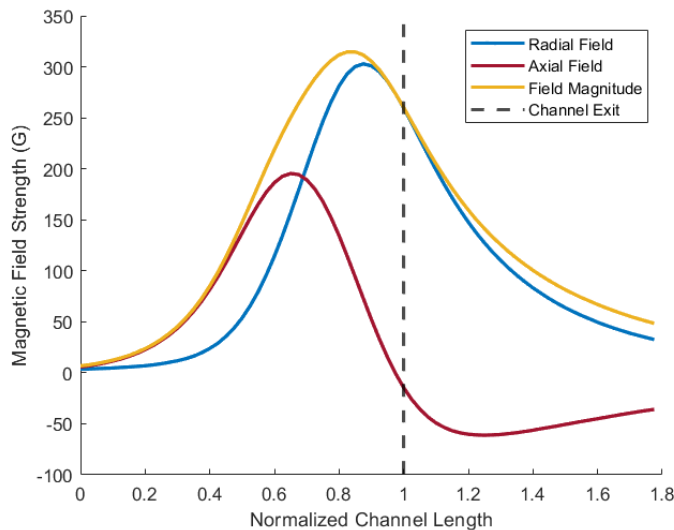


Fig. 6 Channel Center-line Magnetic Field Strength

As desired, the field increases in strength from anode to exit. We also observe that at the peak near the exit plane, the field is largely radial, as required to trap electrons in their cyclotron orbits and induce the $\mathbf{E} \times \mathbf{B}$ drift. The maximum field strength at the exit plane predicted in the 3-Dimensional COMSOL simulation was approximately 330 G. This agrees well with the measured maximum field magnitude of approximately 315 G. From the measured field, we also see a large axial component, peaking around 0.6L. An axial field in the channel is undesirable, as it does not serve to inhibit electron motion to the anode. If electrons are allowed to travel uninhibited from cathode to anode, it may short circuit the discharge and prevent ionization in the channel. Despite this axial component, the field near the channel exit still serves to confine electrons, allowing the thruster to induce a Hall current and create a discharge.

B. Channel

The Hall thruster channel is responsible for containing the plasma and insulating critical components of the thruster such as the magnets. Channel dimensions were based in part on the scaling laws discussed in Section III.E, as well as magnetic field simulation results. To choose the appropriate material for the channel, we performed a trade study, weighing several viable options. The most common material choice for Hall thruster channels is boron nitride. Boron

nitride is typically favored for its thermal and electrical insulating properties, its low susceptibility to sputtering and its low secondary electron emission [5]. However, boron nitride is also expensive, and therefore, was not a viable option for our use case. In considering several other materials, we wanted to favor an option that was thermally and structurally durable and relatively inexpensive. Based on these parameters, we opted for an aluminum channel, coated in boron nitride spray for additional thermal and electrical insulation from the thruster body. While stainless steel also satisfied our trade requirements, the machining difficulty of stainless made it unrealistic. While aluminum does present durability challenges, particularly when considering thermal loads, this thruster is not intended to be run for prolonged testing more than a few hours. Additionally, since this is a demonstration device, it can easily be modified or remade if the channel experiences excess wear in the future.

C. Anode

1. Design and Construction

The anode is responsible for maintaining the axial electric field within the thruster channel. Additionally, our anode was designed to distribute the propellant into the channel by incorporating a plenum and injector face into the architecture. Traditionally, thruster anodes are made of austenitic stainless steel alloys. These materials are readily available and machinable, while also able to withstand the high plasma temperatures at the anode face. Austenitic alloys are non-magnetic as to avoid interfering with the overall thruster magnetic circuit. Therefore, we designed our anode to be made of 304 stainless steel, and to be manufactured in two pieces. The top face acted as an injector plate to evenly distribute neutral gas throughout the channel in hopes of achieving uniform ionization. This injector face had 24 evenly spaced holes, each 0.05" in diameter. This hole diameter was chosen in part because it is the limit of cutting precision on the waterjet. The bottom portion of the anode contained a groove for gas flow, as well as two 1/8" holes for propellant inlet lines. The top and bottom pieces of the anode were designed to be welded together and the propellant lines would be brazed in place to create the final anode/gas distributor assembly. Because manufacturability was a primary design consideration for this anode, we opted for this single plenum design, expecting some shortcomings in the neutral flow distribution. Indeed, more complex anode geometries do exist that contain internal baffles and are more effective at distributing neutral propellant in the channel. However, for the sake of this demonstration unit, the compromise was made to work with an anode that could be easily and quickly manufactured rather than emphasizing optimal gas distribution. A cross section of the anode can be seen at the base of the channel in Figures 2 and 8.

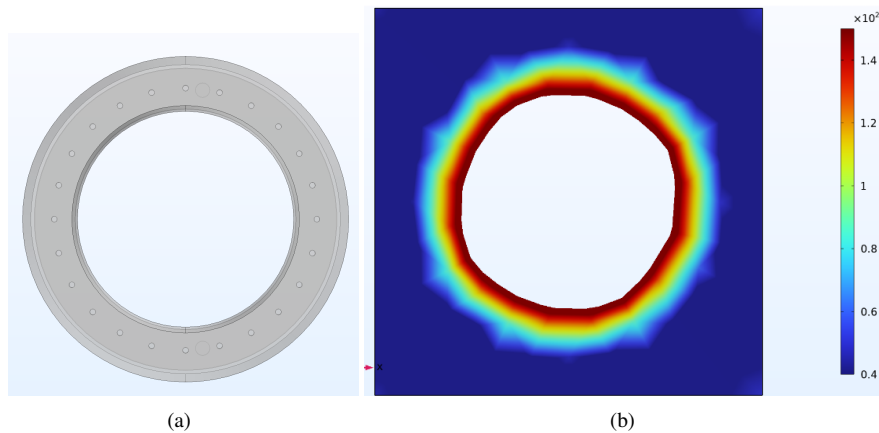


Fig. 7 (a) Anode Flow Model Through Channel, (b) Simulation of Neutral Density at the Channel Exit

2. Flow Simulation

The anode not only supplies the axial electric field within the channel, it also acts as a gas distributor that injects neutral propellant into the channel to be ionized. The goal of the gas distribution scheme is to disperse neutral flow as uniformly as possible, avoiding any local "hot spots" of ionization. To verify this, we used a COMSOL flow simulation of neutrals through the anode into the channel. A flow path CAD model was made to capture the motion through the anode and

into the channel; a top view of the flow path is shown in Figure 7. Due to the fact that the thruster will be running under vacuum, characterizing the flow out of the anode is a complex task. The neutral flow transitions several flow regimes before reaching the ionization region of the channel. Previous work modeling the neutral flow through Hall thruster channels has modeled the flow as molecular [14], therefore the molecular flow module was used in COMSOL. The flow through the anode was set to 50 SCCM, which is the upper end of our expected operating flow rates based on previous operation of the PEPL-70. The free molecular flow module allowed us to visualize the neutral density at the exit plane. For an anode that evenly distributes the flow, we would expect the neutral density to be uniform (one solid color) and symmetric. As we can see from the results shown in Figure 7, the flow path lacks some uniformity and symmetry, however, it generally succeeds at dispersing the flow throughout the channel. Additionally, the neutral densities match published analyses for anodes with similar flow rates. [15]. More complex anode geometries certainly could be chosen to better distribute the neutral flow field. However, this anode design is easily machinable and relatively simple, making it the most accessible option for our purposes.

D. Cathode

As discussed in Section III.A, a hollow cathode is an integral part of Hall thruster operation. For our thruster, we utilized a heaterless LaB₆ hollow cathode that was previously used for the PEPL-70. This cathode had been successfully operated several times on argon prior to this project and had been confirmed to work at the background pressures typical for the vacuum facility used. The cathode was externally mounted and oriented radially inward near the channel exit plane. Typically, the cathode would light at approximately 20 SCCM and 300 V when operating on argon gas. After lighting, cathode flow rate and voltage were decreased slightly; however, the keeper voltage was kept on to at least 100 V even after the main thruster discharge was lit. This was done because testing showed that the thruster would potentially blink out if the keeper voltage was completely turned off. Throughout the described test campaign, the cathode repeatedly and reliably lit on argon and was able to ignite the thruster.

E. Thruster Assembly

With each individual component designed, an assembly was created to ensure proper part alignment and placement. To electrically isolate the channel and anode from the iron base, pieces of ceramic were inserted at the junction between the iron and the channel and over the anode propellant lines. Additionally, to help secure all thruster components, a shaft collar and spring loaded washer combination were placed behind the propellant tubes to the anode. The CAD assembly of the thruster is shown in Figure 8. For thermal considerations, small tolerances were left at joints between dissimilar materials. This helped to ensure that no unwanted electrical or thermal contact would be made as materials underwent thermal expansion during thruster operation.

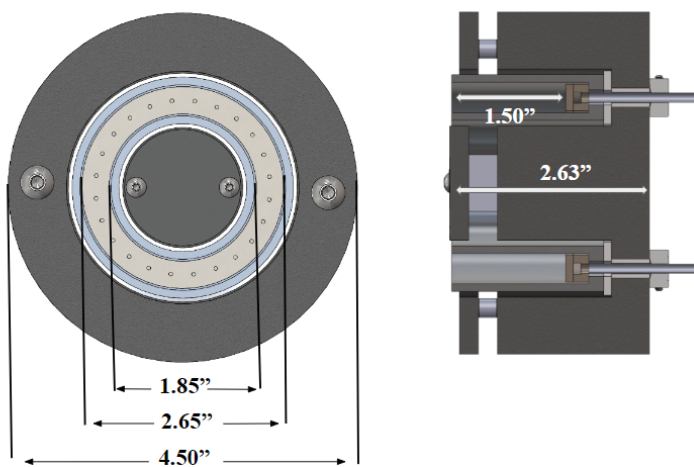


Fig. 8 Thruster Assembly Front and Cross Section Views with Key Dimensions

To manufacture the thruster components, two primary methods were used. Parts with less than 1 inch thickness, such as the anode assembly, iron top plates, and ceramic insulation were designed with the intention of being manufactured

using the water jet. Larger components, such as the channel and the iron base, required CNC machining, which was outsourced to the U-M Literature, Science, and the Arts (LSA) Machine Shop.

1. Water Jet Components

Water jetting is an accessible method of manufacturing that can be used for a variety of materials. For this project, we were able to use two different water jets. The first was the student operated water jet in the University of Michigan Ford Robotics Building, which is completely student-run, and was used to manufacture the iron top plates and the ceramic base. Because the anode components were made of stainless steel, they required a more powerful water jet. Therefore, the anode parts were outsourced to the University of Michigan Taubman water jet. After being water jetted, the two pieces of the anode assembly shown in Figure 9 were welded together in the Wilson Student Team Center.



Fig. 9 Anode Top and Bottom After Water Jetting

2. Machined Components

Due to the depth of the annular channel and iron base, we were unable to machine these components by hand. Therefore, these parts were outsourced to the University of Michigan LSA Machine Shop to be manufactured on a CNC machine.

3. Final Assembly

After all components were manufactured, the thruster was assembled. The anode and channel nested into the iron base and were secured at the back of the thruster using the aforementioned shaft collars and washers on the propellant lines. The magnets were secured in place using fasteners on the iron front plates.

V. Experimental Setup

For testing, it was desired to achieve steady-state operation on argon propellant with a target power of approximately 200 W. Several variables were controlled to adjust the thruster's operating conditions. These included the discharge voltage in volts, as well as anode and cathode mass flow rate in standard cubic centimeters per minute (SCCM). A virtual interface was designed in LabView to enable control inputs for multiple variables to be commanded from a single control panel.

A. Vacuum Chamber Facility

The PEPL MAISE chamber was the facility used to test this thruster. Using a Pfeiffer TPU 1501 turbo-molecular pump, the chamber can achieve a minimum background pressure on the order of 10^{-4} Torr. While this pressure is significantly higher than would be desired for precision testing of a Hall thruster, the mobility and operability afforded by limiting the pumping infrastructure of the chamber is crucial in enabling this system to be a mobile demonstration unit. Additionally, the chamber includes a large, acrylic end cap for viewing of the thruster when in operation. The thruster assembly and cathode were mounted in the chamber using an aluminum 80/20 stand that interfaced with the iron base of the thruster. A picture of the test facility, along with the view of the thruster assembly mounted inside the chamber is shown in Figure 10:

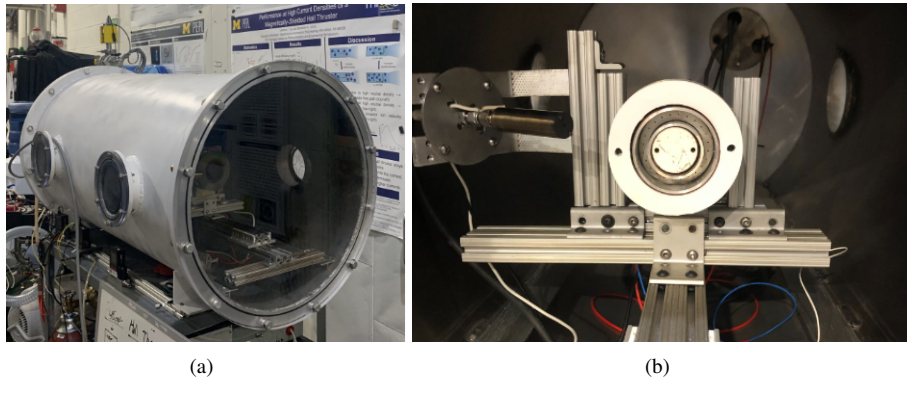


Fig. 10 (a) MAISE Vacuum Chamber and (b) Mounted Thruster Inside the Chamber

B. Controller Setup and Virtual Instrument Interface

The controllable variables that may impact thruster performance include the anode mass flow rate, cathode mass flow rate, and anode voltage. The intention of the control interface was to create a LabVIEW environment capable of providing a single point of command for the devices controlling each of the thruster settings. The notional control flow diagram is shown in Figure 11.

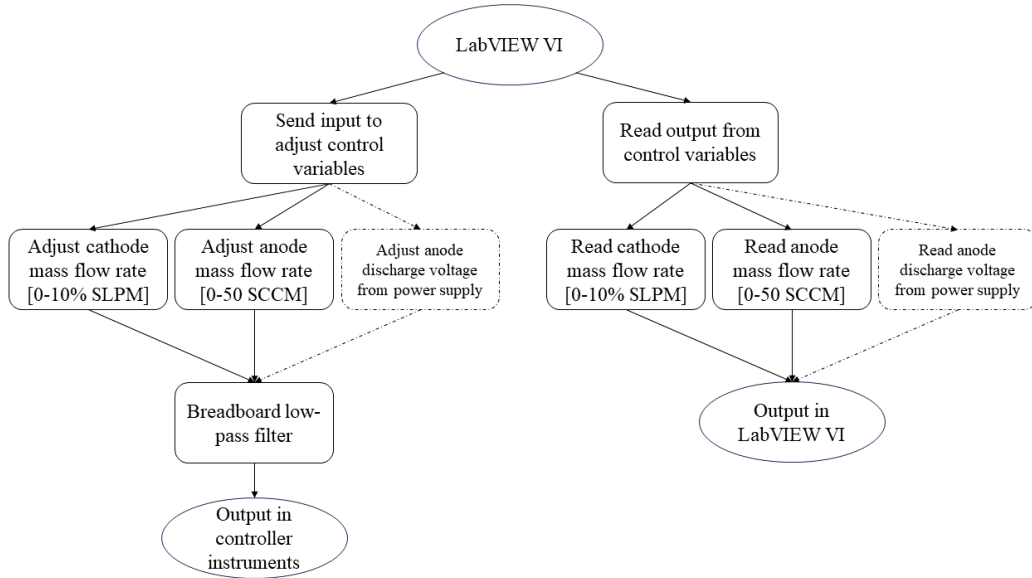


Fig. 11 Control Processes for Adjusting Operating Conditions

The anode was powered by a Sorensen 600 V power supply and the anode and cathode flow were controlled by Alicat mass flow controllers. The control hardware featured an Arduino UNO, which could be used for analog and digital input and output. For changing the flow rates for the anode and cathode, PWM (pulse-width modulation) pins on the Arduino were used to control the power of the electrical signal fed into the specified connection of the pins. This is a common method of sending digital signals that mimic analog signals without a digital-to-analog conversion. The frequency of the PWM pins on the Arduino is 490 Hz. The duty cycle, which is the amount of time the power of the signal is on, and the frequency of the PWM drive the effectiveness of the input signal. During preliminary testing, it was noticed that the duty cycle of the PWM from the Arduino was low, causing the controlled settings of the mass flow controllers and power supply to oscillate. As a remedy, a low pass filter was designed at a cutoff frequency of 1600 Hz to smooth the PWM analog signal. This frequency allows for the mass flow controller to resolve analog signals as a

"DC-like" signal, which enabled us to control the MFCs. A simple setup of the low-pass filter to the Arduino is shown in Appendix B. Unfortunately, when configuring control settings for the power supply, the power input continued to oscillate as an analog signal. Therefore, during testing the power inputs to the thruster were adjusted by hand.

VI. Results

A. Thruster Ignition

Using the MAISE facility and the controllers described in Section V, we tested the thruster at various operating conditions. We found the thruster to reliably ignite at approximately 50 SCCM anode flow, 150 V and 0.5 A. At low currents, a low frequency plasma oscillation was observed as slight flickering in the thruster. Shortly after ignition, the anode flow rate was typically lowered to roughly 25 SCCM. At this point, anode voltage was increased to approximately 200 V and current reached 1 A. This setting appeared to be more stable as the flickering subsided and the plasma appeared visibly more dense, perhaps suggesting more effective ionization. The ignition process was repeated several times with similar results each attempt. The thruster was then allowed to run for an extended test to determine whether the plasma would extinguish itself. The thruster was allowed to run for approximately 1.5 hours before it was determined that steady state was achieved and maintained and the test was concluded. Figure 6 shows the thruster operating at 200 W during an extended test. The purple color of the plasma suggests possible inefficiencies in the ionization process. This may be, in part, due to the high operating pressure in the vacuum chamber, which exceeded 1 mTorr when the thruster was operating. Additionally, from the photos taken of the thruster operating, we qualitatively observe azimuthal non-uniformities in light intensity. This likely is a result of unequal gas distribution through the anode. As discussed, this anode was primarily designed to be manufacturable, so non-uniformities in the gas distribution were to be expected. Additionally, leaks at propellant line interfaces could prevent even flow of neutral gas, which may further exacerbate existing non-uniformities. Inefficiencies aside, the thruster was able to maintain this discharge, making it suitable as a demonstration unit.

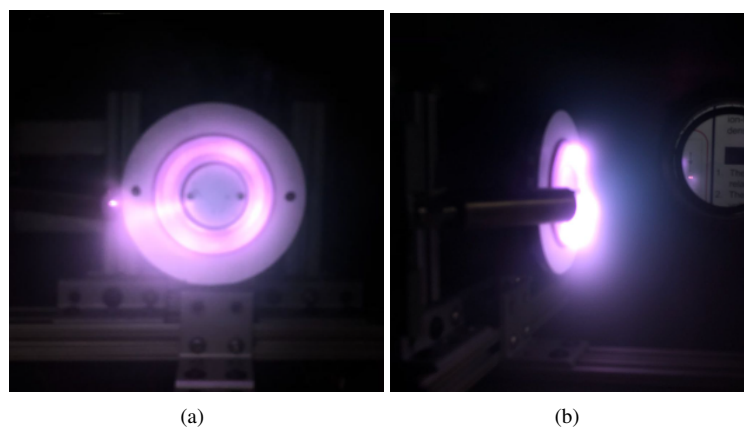


Fig. 12 Front View (a) and Side View (b) of The MAISE Thruster Operating at 200 W on Argon Propellant

B. Channel Erosion

After operating the thruster for a total of approximately five hours, the channel was removed and examined. As shown in Figure 13, erosion was clearly visible close to the exit plane of the channel, approximately at the ionization region. Despite some visible deterioration, the channel was still operable and continued to be used with the thruster. It is probable that the channel will need to be rebuilt in the future and alternative manufacturing methods could enable a more robust material choice for the next iteration.



Fig. 13 Channel Erosion After Five Hours of Operation

VII. Discussion

A. Challenges Encountered

The primary challenge associated with this project was the timeline. Our intention was to completely design, build and test the thruster in a single semester. In reality, due to unforeseen lead times on outsourced machining operations, we were not able to test the thruster until mid-May, several weeks after the semester had ended.

Another area where we encountered difficulty was with our control system. While we were able to interface with the anode and cathode mass flow controllers, the connection was rather unreliable and commands from the computer were not always received properly by the controller. Additionally, we were unable to connect to the thruster power supplies, as the control input signal resulted in undesired fluctuations of the voltage and current. Our troubles with the current likely arise from our use of an Arduino UNO microcontroller. The Arduino PWM pins have a frequency of 490 Hz, which is too low to effectively communicate with the mass flow controllers without the addition of a filter circuit. The signal that was transmitted to the power supply was not able to be resolved properly due to the reliance on the PWM function to generate a smoothed analog signal without having to operate at 100% duty cycle. In the future, a more robust control interface could be designed using a more robust controller such as an OPTO 22 card or any other card that is capable of digital-to-analog conversion.

B. Considerations for Future Work

Although we consider this project to have been largely successful, there are several areas that should be revisited or expanded upon in the future. One component that likely requires redesign is the anode. Given the tight timelines of this project, manufacturability was the primary concern of our anode design. Specifically, we wanted a design that could be waterjetted and subsequently welded. In future works, more complex manufacturing techniques could be utilized to design a multi-baffled anode that more effectively distributes neutral gas into the channel.

Another area that would be interesting to explore in the future is characterization of the thruster at various background pressures. The first step in this effort would be to test the thruster in a higher vacuum environment than the background pressures the MAISE chamber can achieve. PEPL has facilities capable of achieving sub-microTorr background pressures, nearly two orders of magnitude lower than the MAISE chamber. We expect thruster behavior to change dramatically in lower background pressures where phenomena such as neutral collisions are less frequent. If the thruster continues to operate reliably at lower pressures, it would be interesting to perform plasma diagnostic measurements to provide a quantitative understanding of the device's behavior.

Finally, because this device was designed to be a demonstration unit, the primary consideration for the future should be showing the thruster to an uninformed audience. Since its construction, the thruster has been displayed during multiple

tours of PEPL, mostly to other engineers. However, as the MAISE team continues to work, the near-term goal is to display the thruster at future outreach events for K-12 students, inspiring them to think about careers in STEM.

VIII. Conclusion

The Hall-Effect Thruster designed in this paper aimed to replace PEPL-70, the current Hall thruster used by MAISE for demonstration purposes. The fundamental design of our thruster was based on scaling laws to determine electron and ion Larmor radii, ionization region, and channel length. Based on these constraints it was determined that the range of suitable magnetic fields ranged from 60 G-1800 G, with a desired field strength of 200-300 G. For the final 3-D model, the magnetic field strength was simulated to be 330 G. Furthermore, based on scaling laws for argon, the channel length was determined to be 1.5 inches. COMSOL Multiphysics was then used to support an iterative design process through a 2-D radial simulation to solidify magnet dimensions and sizing. The software was also used to validate the anode design using a maximum expected anode flow rate of 50 SCCM.

In tandem with the iterative magnetic field analysis, the physical design of the thruster was modeled in Solidworks with three main goals: directing magnetic field lines radially across the channel while maintaining field strength, providing insulation from the plasma in the channel, and properly distributing the argon gas propellant into the channel. To address the magnetic field lines, iron was chosen due to its high magnetic permeability. Two iron plates were designed above the inner and outer magnets to guide the field lines across the channel. Ideally, a boron nitride channel would provide the best insulating properties, but due to its cost and machining difficulties, an aluminum channel with a boron nitride spray coating was used. For the anode design, based on heritage, stainless steel alloys were used to manufacture a top injector plate used to distribute the neutral gas propellant evenly throughout the channel. Additionally, a bottom plate provided a channel for gas flow and two holes for the propellant inlet. These components were manufactured using a combination of water jetting and CNC machining and the two parts of the anode were welded together. After manufacturing, the thruster was assembled.

A magnetic field map was taken of the thruster center line. The experimental mapping showed good agreement with the simulated magnetic field, with a measured peak field strength of roughly 315 G near the thruster exit. The mapping also revealed a strong axial component that existed in the magnetic field at about the half length of the channel. While this axial field suggested possible instabilities, the overall field was deemed suitable since it maintained the desired radial shape in the ionization region. To test, the thruster was mounted inside the PEPL MAISE vacuum facility and a pre-existing hollow cathode was used. We were able to demonstrate extended operation on argon propellant, running at an input power of 200 W and an anode mass flow rate of 25 SCCM. After operating the thruster several times, the channel was examined and erosion was clearly visible. This suggests a possible need to remake the channel out of a more robust material in the future.

In completing this project, we demonstrated that a group of undergraduates with minimal prior experience in EP can successfully design, build, and test a Hall thruster in one semester. By utilizing accessible materials and manufacturing techniques, we were able to complete this design cycle quickly and affordably. The total project cost was less than \$2000, which is reasonable for many student groups. An itemized budget is shown in Appendix A. Since its completion, this thruster has been used at several tours of PEPL and will continue to be used as a demonstration unit in the future. The thruster also provides a platform for future undergraduates who may be interested in working on electric propulsion technologies.

Acknowledgments

We would like to express our gratitude to Professor Benjamin Jorns, our supervisor throughout this project. We are very grateful that he provided us with this research opportunity and we have learned a great deal from it.

We would also like to thank William Hurley and Tate Gill for their invaluable contributions to this project. Their expertise and guidance have been essential for our success.

Lastly, we would like to provide special thanks to Abhiram Kondur for his supervision on the water jet, as well as Cameron Crandall and Jack Taliercio for their assistance in welding thruster components.

References

- [1] Baird, M. J., "Designing an Accessible Hall Effect Thruster," Ph.D. thesis, Western Michigan University, 2016.
- [2] Baird, M. J., Simmons, N. A., and Lemmer, K. M., "Performance characterization of a small low-cost Hall thruster," *35th International Electric Propulsion Conference*, 2017.
- [3] Oh, B., Kunimune, J., Spicher, J., and Anfenson, L., "Undergraduate Demonstration of a Hall Effect Thruster: Self Directed Learning in an Advanced Project Context," *ASEE'S Virtual Conference*, Vol. 29672, 2020.
- [4] Oh, B., and et. al., "Design, fabrication, and testing of an undergraduate hall effect thruster," *Journal of Electric Propulsion*, Vol. 2,6, 2023.
- [5] Goebel, D. M., and Katz, I., *Fundamentals of Electric Propulsion: Ion and Hall Thrusters*, JPL Space Science and Technology Series, Wiley, 2008.
- [6] Raitses, Y., Smirnov, A., Staack, D., and Fisch, N. J., "The Dependence of the Electron Temperature on the Discharge Voltage for Different Hall Thruster Configurations," *29th International Electric Propulsion Conference (IEPC)*, Princeton University Plasma Physics Laboratory, Princeton, NJ, 08543, 2005.
- [7] Y. Raitses, A. S., and Fisch, N. J., "Effects of Enhanced Cathode Electron Emission on Hall Thruster Operation," *Physics of Plasmas*, Vol. 16, 2009.
- [8] Vacuum, P., "Thermal Velocity," , 2023. URL <https://www.pfeiffer-vacuum.com/en/know-how/introduction-to-vacuum-technology/fundamentals/thermal-velocity/>.
- [9] Naoya Kuwabara, N. Y., Masatoshi Chono, and Kuwahara, D., "Electron Density Measurement inside a Hall Thruster Using Microwave Interferometry," *Journal of Propulsion and Power*, Vol. 37, No. 3, 2021, pp. 491–494. <https://doi.org/10.2514/1-b38163>.
- [10] Goebel, D. M., and Katz, I., "Appendix E: Ionization and Excitation Reaction Rates for Xenon in Maxwellian Plasmas," *Fundamentals of Electric Propulsion: Ion and Hall Thrusters*, JPL Space Science and Technology Series, Wiley, 2008, pp. 475–477.
- [11] Rapp, D., and Englander-Golden, P., "Total Cross-Sections for Ionization and Attachment in Gases by Electron Impact. I. Positive Ionization," *The Journal of Chemical Physics*, Vol. 43, No. 5, 1965, pp. 1464–1479. <https://doi.org/10.1063/1.1696957>.
- [12] Solutions, I. M., "Samarium Cobalt vs Neodymium Magnets," , 2023. URL <https://idealmagnetsolutions.com/knowledge-base/samarium-cobalt-vs-neodymium-magnets/>.
- [13] Technologies, A. M., "Samarium Cobalt vs. Neodymium Iron Boron," , 2023. URL <https://www.arnoldmagnetics.com/resources/samarium-cobalt-vs-neodymium-iron-boron/>.
- [14] Xu, Z., "Effect of azimuthal diversion rail on an ATON-type Hall thruster," *The Journal of Applied Physics*, Vol. 50, No. 095202, 2016.
- [15] Haotian, F., "Discharge characteristics of Hall thruster with large height-radius ratio," *Acta Astronautica*, Vol. 185, 2021, pp. 206–214.

Appendix A: List of Components and Total Cost

Table 1: Hall-Effect Thruster Materials List.

Item	Size	Quantity	Cost	Supplier/Manufacturer
304-Stainless Steel Stock	4" x 4"	1	\$133.23	Midwest Steel Supply
Aluminum Silica Ceramic	4" x 4" x 1/8"	2	\$70.26	McMaster-Carr
Ductile Iron Stock	5" x 6"	1	\$201.45	McMaster-Carr
Boron Nitride Spray Coating	—	1	—	PEPL
Ceramic Standoff	1/4" x 1/4"	4	\$14	McMaster-Carr
SmCo Grade 26 Outer Magnet	0.25" diameter 0.25" thickness	12	\$71.16	Magnetshop
SmCo Grade 26 Inner Magnet	0.75" diameter 0.375" thickness	2	\$131.74	Magnetshop

Table 2: Total Cost of Project.

Item	Cost
Materials	\$621.84
LSA Manufacturing Shop	\$1268
Water Jet	\$68
Total Cost:	\$1957.84

Appendix B: RC Filter Setup

An RC low-pass filter is characterized by its cutoff frequency, which is the frequency where high-frequency signals begin to be attenuated. The cutoff frequency f_c is dependent on the resistance and capacitance, represented in Equation 10:

$$f_c = \frac{1}{2\pi RC} \quad (10)$$

A 1 kΩ resistor and 100 pF capacitor were chosen to generate a cutoff frequency of about 1600 Hz, which is 3 times faster than the Arduino UNO PWM frequency, allowing for a smoother analog DC signal. The Bode plot for the response curve of the chosen low-pass filter at a DC gain of 1 is shown in Figure 14. The filter is a simple breadboard circuit, shown in Figure 15, that connects to the Arduino microcontroller, which interfaces with the local LabVIEW GUI to configure the control settings of the mass flow controllers for the anode and cathode.

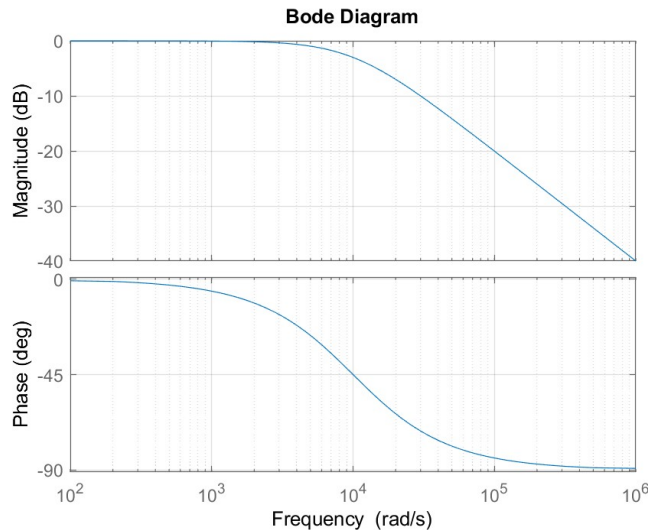


Fig. 14 RC Low-pass Filter (1600 Hz Cutoff Frequency) Bode Plot.

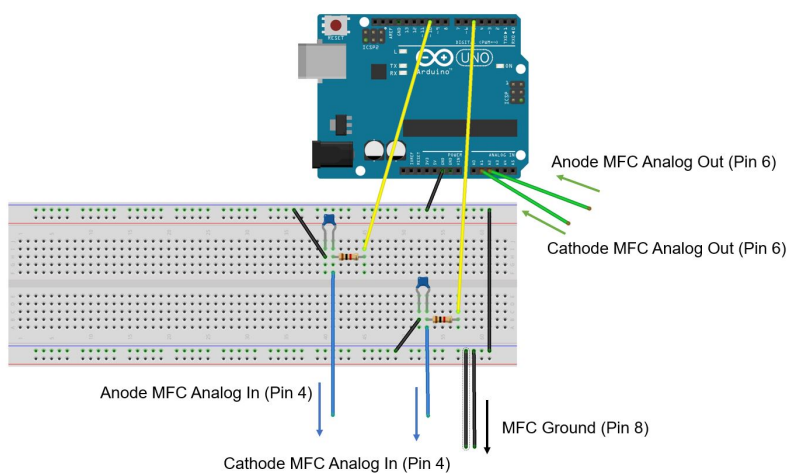


Fig. 15 Hardware Setup For RC Filter and Arduino Interface With MFCs.